Transport coefficients of the Lennard-Jones model fluid. II Self-diffusion

Karsten Meier[a)]
Institut für Thermodynamik, Helmut-Schmidt-Universität—Universität der Bundeswehr Hamburg, Holstenhofweg 85, D-22043 Hamburg, Germany

Arno Laesecke
Physical and Chemical Properties Division, Chemical Science and Technology Laboratory, National Institute of Standards and Technology, Boulder, Colorado 80305

Stephan Kabelac
Institut für Thermodynamik, Helmut-Schmidt-Universität—Universität der Bundeswehr Hamburg, Holstenhofweg 85, D-22043 Hamburg, Germany

(Received 19 May 2004; accepted 2 July 2004)

In an extensive computer simulation study, the transport coefficients of the Lennard-Jones model fluid were determined with high accuracy from equilibrium molecular-dynamics simulations. In the frame of time-correlation function theory, the generalized Einstein relations were employed to evaluate the transport coefficients. This second of a series of four papers presents the results for the self-diffusion coefficient, and discusses and interprets the behavior of this transport coefficient in the fluid region of the phase diagram. The uncertainty of the self-diffusion data is estimated to be 1% in the gas region and 0.5% at high-density liquid states. With the very accurate data, even fine details in the shape of the self-diffusion isotherms are resolved, and the previously little-investigated behavior of the self-diffusion coefficient at low-density gaseous states is analyzed in detail. Finally, aspects of the mass transport mechanisms on the molecular scale are explored by an analysis of the velocity autocorrelation functions. © *2004 American Institute of Physics.*
[DOI: 10.1063/1.1786579]

I. INTRODUCTION

This is the second of a series of four papers that report the results of an extensive molecular-dynamics simulation study on the transport coefficients of the Lennard-Jones model fluid.[1,2] Here, the results for the self-diffusion coefficient are presented. The results for the viscosity have been discussed in a preceding paper[3] referred to hereafter as paper I, and subsequent papers deal with the bulk viscosity[4] and thermodynamic properties.[5]

The self-diffusion coefficient is a measure for the diffusion of a particle in a pure fluid. Experimental studies on the self-diffusion coefficient of real fluids are scarce since it is difficult to measure the diffusion of a particle in surrounding particles of the same species. Available data sets cover few substances and only limited portions of the fluid region. Examples are the studies of Trappeniers and co-workers[6] on methane, xenon, and ethene, of Lüdemann and co-workers[7] on halogenated hydrocarbons, of Peereboom *et al.*[8] on xenon, and of Harris[9] on methane. In molecular-dynamics simulations, self-diffusion coefficients can be determined conveniently and with high accuracy. Therefore, this transport coefficient was subject of many simulation studies. A review of available literature data for the hard sphere, square-well, and Lennard-Jones model fluids was given by Liu *et al.*[10]

It will be shown later in this paper that data for the self-diffusion coefficient exhibit a strong dependence on the number of particles in the simulated system. As many literature data were obtained from simulations of relatively small systems with typically 500 or less particles, they are expected to be subject to systematic errors. Since the simulations of this work were carried out with 1372 particles, the present results approximate the true infinite-system size values more closely than most currently available literature data. Moreover, many previous studies on the self-diffusion coefficient focused on the liquid region. The present work explores in addition the previously little-investigated low-density gaseous states.

This paper is organized as follows: The following section provides the theoretical background for the calculation of the self-diffusion coefficient in equilibrium molecular-dynamics simulations and describes the simulation procedure and analysis of the results. Section III presents an investigation of the influence of simulation parameters on the results for the self-diffusion coefficient. In Sec. IV, the self-diffusion data are discussed and compared with literature data. In Sec. V, the temperature and density dependence of the self-diffusion coefficient are examined. Finally, an interpretation of the self-diffusion coefficient in Sec. VI in terms of velocity autocorrelation functions gives some insights into the mass transport mechanisms on the molecular scale.

II. SIMULATION PROCEDURE

There are two different approaches to calculate the self-diffusion coefficient by molecular-dynamics simulations: either by nonequilibrium molecular dynamics or by time-

a)Electronic mail: karsten.meier@hsuhh.de

correlation function theory employing the Green–Kubo integral formula or Einstein relation in equilibrium simulations. The latter methods are usually preferred because they yield self-diffusion data with much higher accuracy.

In time-correlation function theory, the self-diffusion coefficient D is given by the Green–Kubo integral formula[11]

$$D=\frac{1}{3(N-1)}\sum_{i=1}^{N}\int_0^\infty \langle \mathbf{v}_i(t)\cdot\mathbf{v}_i(t_0)\rangle \mathrm{d}t \tag{1}$$

or, equivalently, by the Einstein relation[11]

$$D=\lim_{t\to\infty}\frac{1}{6(N-1)}\sum_{i=1}^{N}\frac{d}{dt}\langle[\mathbf{r}_i(t)-\mathbf{r}_i(t_0)]^2\rangle. \tag{2}$$

In these equations, N stands for the number of particles, $\mathbf{r}_i$ and $\mathbf{v}_i$ are the position and velocity vector of particle i, and t is time. The angular brackets indicate an equilibrium ensemble average over short trajectory sections of the phase-space trajectory of the system with time origins t_0. In both cases, averaging over all particles is used to reduce the statistical uncertainty of the self-diffusion data. The Green–Kubo integral formula determines the self-diffusion as the integral of the velocity autocorrelation function, whereas the Einstein relation relates it to the slope of the mean-squared displacement of the diffusing particle in the long-time limit $t\to\infty$. The factors $N-1$ take into account that only $N-1$ particle velocity and position vectors are independent in the molecular-dynamics ensemble at constant NVE**MG**,[12] in which the present simulations were carried out. From a mathematical point of view, both the Green–Kubo integral formula, Eq. (1), and the Einstein relation, Eq. (2), are completely equivalent[11] and could in principle be used to determine the self-diffusion coefficient. In this work, the Einstein relation method was chosen because particle positions are more accurately obtained from the integration of the equations of motion than are particle velocities.[13]

The self-diffusion data were derived from the same simulations from which the viscosity data reported in paper I were obtained. All simulations were carried out in the classical molecular-dynamics ensemble at constant NVE**MG** as described in paper I. At every simulated time step, the instantaneous properties of the system were calculated and stored. Particle positions and velocities were stored in regular intervals. After a simulation run, several separate analysis programs were used to compute thermodynamic state variables, time-correlation functions, and generalized mean-squared displacement functions from the stored data. Mean-squared particle displacements were calculated from unfolded particle trajectories, from which the periodic boundary conditions were removed.[14] In a subsequent analysis step, the self-diffusion coefficients were obtained from a careful analysis of the Einstein relations and velocity autocorrelation functions by the same procedure as described in paper I for the viscosity and the shear-stress autocorrelation functions.

In the remainder of this paper, reduced quantities denoted by a superscript asterisk "*" are used, e.g., $T^*=Tk/\varepsilon$, $\rho^*=\rho\sigma^3$, $t^*=t\sqrt{\varepsilon/m}/\sigma$, $r^*=r/\sigma$, $\mathbf{v}^*=\mathbf{v}\sqrt{m/\varepsilon}$, and $D^*=D\sqrt{m/\varepsilon}/\sigma$, where ε and σ are the energy and length scaling parameters of the Lennard-Jones potential, and m is the particle mass.

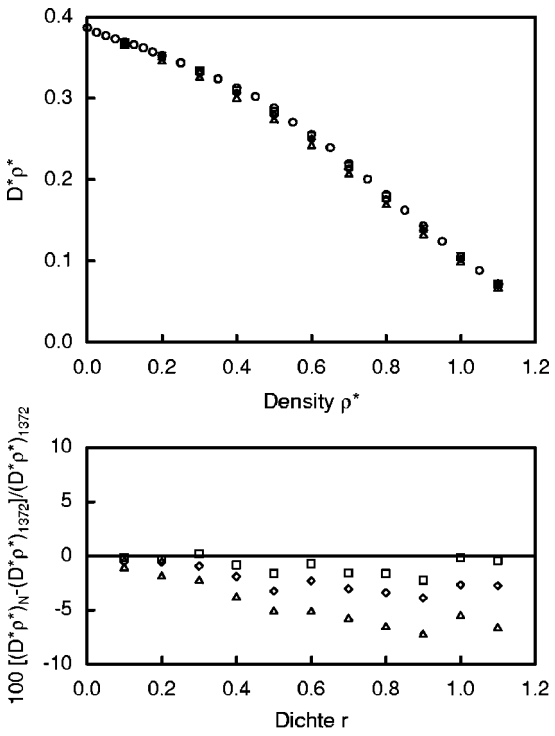

FIG. 1. $D^*\rho^*$ along the isotherm $T^*=3.0$ as a function of the density for different numbers of particles N. Simulation parameters: (○) $N=1372$, $r_{\mathrm{cut}}^*=5.0$–6.5, 10^6 time steps; (□) $N=864$, $r_{\mathrm{cut}}^*=3.0$, 3×10^6 time steps; (◇) $N=500$, $r_{\mathrm{cut}}^*=3.0$, 6×10^6 time steps; (△) $N=256$, $r_{\mathrm{cut}}^*=3.0$, 10×10^6 time steps.

In the discussion of the self-diffusion data, the product self-diffusion coefficient times density $D^*\rho^*$ is considered rather than the self-diffusion coefficient itself. The self-diffusion coefficient tends to infinity in the zero-density limit, where the mobility of the particles is not restricted by surrounding molecules. Since this singularity is of order 1, it can be removed by multiplying the self-diffusion coefficient with density. $D^*\rho^*$ remains finite in the zero-density limit and takes the values known from the Chapman–Enskog solution to the Boltzmann equation.[15]

III. INFLUENCE OF SIMULATION PARAMETERS ON THE SELF-DIFFUSION DATA

Any simulation result is subject to statistical and systematic errors. Statistical errors in simple simulation averages were estimated by the method described by Allen and Tildesley,[13] which is originally due to Friedberg and Cameron.[16] Systematic errors can be eliminated to some extent by a careful choice of the simulation parameters. Since it is not *a priori* known how the simulation parameters, e.g., cutoff radius, and number of particles, must be chosen, a systematic investigation of their influence on the results for macroscopic properties is required.

The influence of the cutoff radius on the results for $D^*\rho^*$ was investigated at the state point ($T^*=0.722$, $\rho^*=0.8442$) close to the triple point of the Lennard-Jones

TABLE I. Literature data sets for the self-diffusion coefficient of the Lennard-Jones model fluid. Abbreviations: CC, constant color current method; CG, constant color current gradient method; ER, Einstein relation method; GK, Green–Kubo integral method; MC-GO, Monte Carlo generated time origins.

Author	Year	Data	Method	Ensemble	N	r_{cut}^*	T^*	ρ^*	Simulation length[a]
This work	2004	334	ER	*NVE***MG**	1372	5.5–6.5	0.7–6.0	0.005–1.275	4500–6000
Borgelt (Ref. 19)	1990	46	GK	*NVE***MG**	108	2.5	0.66–2.94	0.78–0.84	371
Canales (Ref. 20)	1999	3	GK/ER	*NVT*	668	2.71–3.11	0.53, 1.89	0.756, 1.143	554–1203
Chen (Ref. 21)	1977	6	ER	*NVE***MG**	500	2.5	0.679–2.16	0.3–0.8442	23–35
Erpenbeck (Ref. 22)	1987	4	GK	*NVT*	108–1372	1.74[b]	1.08	0.85	MC-GO
		3	CC	*NVT*	108–1372	1.74[b]	1.08	0.85	32–932
Erpenbeck (Ref. 23)	1988	6	GK	*NVT*	108–4000	2.75[b]	0.722	0.8442	MC-GO
		2	GK	*NVT*	108, 864	2.75[b]	0.722	0.8442	MC-GO
Gardner (Ref. 24)	1991	22	ER	*NVE***MG**	108, 256	$L/2$	1.3, 2.49	0.01–0.3	10 000
Hammonds (Ref. 25)	1988	53	GK	*NVE***MG**/*T*	108–500	2.5[c]	0.72–10.0	0.4–1.18	3000–14 000
Heyes (Ref. 26)	1983	54	ER	*NVE***MG**	256	2.5	0.68–4.58	0.2–1.13	150
Heyes (Ref. 27)	1987	16	ER	*NVT*	108–2048	[d]	1.4562	0.1–1.0	100–9000
Heyes (Ref. 28)	1988	213	ER	*NVT*	108–500	[d]	0.72–10.0	0.2–1.22	417–9500
Heyes (Ref. 29)	1990	26	GK	*NVT*	256	2.5	0.722–6.0	0.4–1.4	1500
Heyes (Ref. 30)	1993	4	GK	*NVE***MG**	256	2.5	0.707–6.0	0.5–1.0	655–17 082
Kincaid (Ref. 31)	1994	6	CG/ER	*NVE*	256–1372	1.24[b]	2.0	0.05–0.5	ER: 2200–30 000
Leegwater (Ref. 32)	1991	7	GK	[d]	500	[d]	0.84–1.96	0.2–0.85	[d]
Michels (Ref. 33)	1975	22	GK	*NVE***MG**	125	2.5	1.5–3.0	0.04–0.35	
Michels (Ref. 34)	1978	43	GK	*NVE***MG**	108, 125	2.5	1.3–5.56	0.01–0.3	306–28 850
Rowley (Ref. 35)	1997	141	ER	*NVT*	256	3.5	0.8–4.0	0.05–1.0	182–6063
Schofield (Ref. 36)	1973	4	GK	*NVE***MG**	[d]	2.25	1.0	0.626–0.845	[d]
Sharma (Ref. 37)	1994	5	GK	*NVT*	32–864	1.6, 2.5	0.72	0.84	80–400
Straub (Ref. 38)	1992	35	ER	*NVE***MG**	512	2.5	0.75–4	0.3–1.05	150

[a]Values of the simulation length are given in reduced time units.
[b]Modified Lennard-Jones potential.
[c]According to Fig. 1 in Ref. 26.
[d]Not reported by the authors.
[e]At least 500 times the half-value of the correlation function.

model fluid, at which the viscosity was examined in paper I. The self-diffusion data showed no significant influence on this simulation parameter at cutoff radii larger than $r_{cut}^* = 4.5$.

In order to examine the dependence of results for $D^*\rho^*$ on the number of particles, several simulation series with different particle numbers were carried out. In Fig. 1, the influence of the number of particles on $D^*\rho^*$ is illustrated for the supercritical isotherm $T^* = 3.0$. $D^*\rho^*$ shows a strong dependence on the number of particles from the density $\rho^* = 0.2$ up to the highest simulated density close to the freezing line. The largest effect, with up to 8% difference between the results for 256 and 1372 particles, is observed at intermediate densities. At gaseous densities below $\rho^* = 0.3$, the dependence of the number of particles decreases and good agreement between the results for 864 and 1372 particles is found. Consequently, with 1372 particles the results for $D^*\rho^*$ at densities $\rho^* \leqslant 0.3$ represent $D^*\rho^*$ for the macroscopic Lennard-Jones model fluid well. However, at higher densities the macroscopic values for $D^*\rho^*$ are expected to be still higher than the results for 1372 particles.

IV. RESULTS FOR THE SELF-DIFFUSION COEFFICIENT

For the determination of the transport coefficients of the Lennard-Jones model fluid over a wide range of fluid states, extensive equilibrium molecular-dynamics simulations were carried out along 16 isotherms on 351 state points, from which 334 self-diffusion data were derived. Details of these simulations and the distribution of the simulated state points were already described in paper I. The simulations extend over a wide range of the fluid region of the phase diagram from the low-density gas to the compressed liquid close to the freezing line and cover the temperature range between $T^* = 0.7$ and 6.0. At every simulated state point, several thermodynamic state variables, and the transport coefficients' viscosity, bulk viscosity, and the self-diffusion coefficient, were evaluated. While this paper discusses the self-diffusion coefficient, the results for the viscosity were reported in paper I and two subsequent publications treat the bulk viscosity and thermodynamic properties.

At every simulated state point, mean-squared particle displacements and velocity autocorrelation functions were computed. The parameters for the computation of these functions depend on the state point. At densities above $\rho^* = 0.2$, the coordinates and velocities of the molecules were stored every tenth time step during the first million time steps of the production phase of the simulation. Time origins were taken at every 20th time step. At lower densities, the coordinates and velocities were stored every 20th time step during the first 1.5×10^6 time steps for the isotherm $T^* = 1.2$ and higher temperatures. At lower temperatures, they were stored during the whole production phase of the simulation over 2×10^6 time steps. Every 40th time step was taken as a time origin in these cases. The self-diffusion coefficients were determined from the Einstein relation, Eq. (2). The simulation data of this work were deposited as text files in the electronic archive of this Journal[17] and in the electronic archive of the

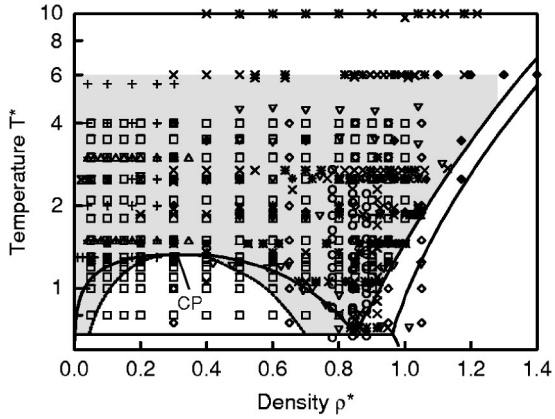

FIG. 2. The distribution of literature data sets for the self-diffusion coefficient in the T^*, ρ^* plane. The gray shaded area is the state region considered in this work. Legend: (○) Borgelt *et al.* (Ref. 19), (⧖) Gardner *et al.* (Ref. 24), (*) Hammonds and Heyes (Ref. 25), (▽) Heyes (Ref. 26), (■) Heyes (Ref. 27), (×) Heyes (Ref. 28), (♦) Heyes and Powles (Ref. 29), (△) Michels and Trappeniers (Ref. 33), (+) Michels and Trappeniers (Ref. 34), (□) Rowley and Painter (Ref. 35), and (◇) Straub (Ref. 38).

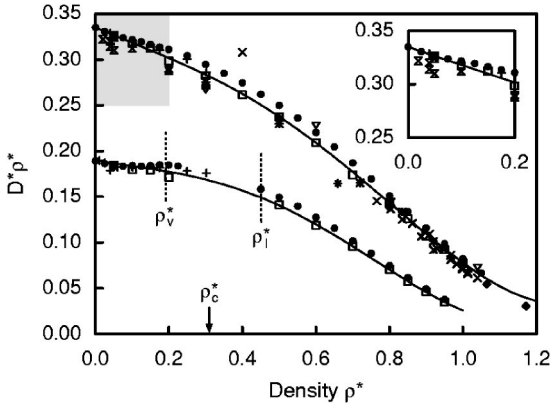

FIG. 3. $D^*\rho^*$ on the subcritical isotherm $T^*=1.3$ and on the supercritical isotherm $T^*=2.5$ as a function of density. The shaded area is enlarged in the inset. Symbols at zero density denote the Chapman–Enskog solution to the Boltzmann equation, and ρ_v^*, ρ_l^*, and ρ_c^* represent the saturated vapor density, saturated liquid density, and critical density, respectively. Legend: (●) This work, (⧖) Gardner *et al.*(Ref. 24), (*) Hammonds and Heyes (Ref. 25), (▽) Heyes (Ref. 26), (×) Heyes (Ref. 28), (♦) Heyes and Powles (Ref. 29), (+) Michels and Trappeniers (Ref. 34), (□) Rowley and Painter (Ref. 35), and (—) correlation of Rowley and Painter (Ref. 35).

NIST Physical and Chemical Properties Division.[18] The statistical uncertainty of the data is estimated to be 0.5% at densities larger than $\rho^*=0.2$, and 1% at lower gaseous densities.

Table I summarizes details of literature data sets for the self-diffusion coefficient of the Lennard-Jones model fluid. In an additional study, Heyes[39] determined the self-diffusion coefficient by equilibrium molecular-dynamics simulations using the Einstein relation method, but the data were not reported in the publication. A critical assessment of the quality of the data sets must take into account the simulation method and parameters employed by the authors.

Most data sets were determined from simulations of systems with 108–500 particles. Exceptions are the data sets of Erpenbeck[22] and Kincaid *et al.*[31] which were obtained from simulations of systems with up to 4000 or 1372 particles, respectively. In the preceding section, it was shown that self-diffusion data depend strongly on the number of particles in the simulated system. It must be expected that the literature data are also subject to this effect.

The data sets of Erpenbeck[22] and Kincaid *et al.*[31] were derived from simulations with a modified Lennard-Jones potential, in which the attractive part of the potential was replaced by a cubic polynomial function that decays continuously to zero. This modification of the potential results in macroscopic thermodynamic state variables and transport coefficients that deviate significantly from the corresponding properties of the original potential.[40] Hence, these data cannot be compared with those data sets that are based on the original Lennard-Jones potential.

In the majority of studies, equilibrium molecular-dynamics simulations were employed, and the Einstein relation or Green–Kubo integral methods were used to determine the self-diffusion data. Indicators for the accuracy of the data obtained by these methods are the lengths of the production phases of the simulations and the number of time origins that are used in the calculation of the velocity autocorrelation and mean-squared displacement functions. Since both functions are single particle properties, they are usually averaged over all particles in the system to increase the accuracy of the results. Thus, simulations of large systems with many particles yield data with smaller uncertainties than those carried out with small systems, provided that the simulations extend over comparable time periods and that time origins are taken sufficiently frequent and at equally spaced intervals from the simulated phase space trajectory. Besides the present data, the data sets of Hammonds and Heyes,[25] Heyes,[28,30] Michels and Trappeniers,[34] and Rowley and Painter[35] were obtained from relatively long simulation runs.

Figure 2 shows the distribution of the data sets for the self-diffusion coefficient in relation to the phase boundaries in the T^*, ρ^* plane. The present data cover the temperature range between $T^*=0.7$ up to 6.0 and the density range from low-density gaseous states up the compressed liquid close to the freezing line. The literature data sets concentrate in the high-density liquid region. Similar temperature ranges are covered by the data sets of Hammonds and Heyes,[25] Heyes,[26,28] Heyes and Powles,[29] and Rowley and Painter.[35] The data sets of Hammonds and Heyes[25] and Heyes[28] extend up to the temperature $T^*=10$. Data at low-density gaseous states were reported by Gardner, *et al.*,[24] Michels and Trappeniers,[33,34] and Rowley and Painter.[35]

In Fig. 3, the present simulation results for $D^*\rho^*$ are shown for two selected isotherms, the subcritical isotherm $T^*=1.3$ and the supercritical isotherm $T^*=2.5$. Also included are literature data from different sources discussed above and the correlation of Rowley and Painter.[35] The present data appear very consistent and extrapolate well into the zero-density limit. On the isotherm $T^*=1.3$, a shallow minimum is observed at the approximate density $\rho^*=0.1$ in the gas region. Isotherm $T^*=2.5$, however, does not show such a minimum.

The data of Rowley and Painter[35] also give a consistent picture, but are systematically lower than the present data in

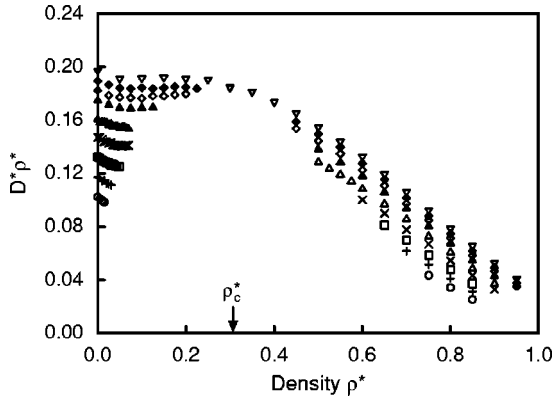

FIG. 4. $D^*\rho^*$ for all simulated subcritical isotherms as a function of density. Symbols at zero density denote the Chapman–Enskog solution to the Boltzmann equation. Legend: (○) $T^*=0.7$, (+) $T^*=0.8$, (□) $T^*=0.9$, (×) $T^*=1.0$, (△) $T^*=1.1$, (▲) $T^*=1.2$, (◇) $T^*=1.25$, (◆) $T^*=1.3$, and (▽) $T^*=1.35$ (supercritical).

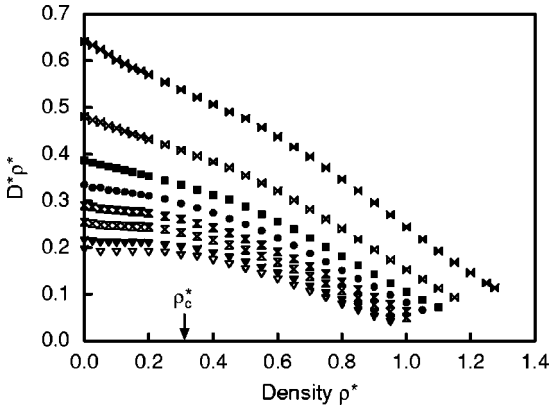

FIG. 5. $D^*\rho^*$ for all simulated supercritical isotherms as a function of density. Symbols at zero density denote the Chapman–Enskog solution to the Boltzmann equation. Legend: (▽) $T^*=1.35$, (▼) $T^*=1.5$, (⧖) $T^*=1.8$, (⧗) $T^*=2.1$, (●) $T^*=2.5$, (■) $T^*=3.0$, (⋈) $T^*=4.0$, and (⧓) $T^*=6.0$.

the liquid region. Since their simulations were performed with 256 particles, and the present simulations with 1372 particles, these systematic deviations are probably due to finite-size effects. The low-density data of Michels and Trappeniers[34] lie between the present data and the data of Rowley and Painter. As their simulations were carried out with 108 and 125 particles, these systematic deviations may also be attributed to finite-size effects. On the other hand, this is surprising because it is expected that self-diffusion data from simulations with fewer particles are smaller than data derived from simulations of large systems. On the isotherm $T^*=2.5$, the literature data sets of Gardner *et al.*,[24] Hammonds and Heyes,[25] Heyes,[26,28] and Heyes and Powles[29] lie mostly below the present data and scatter more. They were derived from simulations with up to 500 particles. The correlation of Rowley and Painter follows their data well at high densities, but fails to describe the correct physical behavior in the gas region.

This discussion shows that the present comprehensive self-diffusion data are substantially more accurate than the literature data on the two isotherms. Similar observations as those reported above were made in comparison to the present data with literature data on other isotherms.[1,2]

V. TEMPERATURE AND DENSITY DEPENDENCE OF THE SELF-DIFFUSION COEFFICIENT

The present results characterize the temperature and density dependence of $D^*\rho^*$ comprehensively and accurately. Figures 4 and 5 display the $D^*\rho^*$ data for all 16 simulated subcritical and supercritical temperatures. Every isotherm extrapolates well into the zero-density limit, and their initial slope is always negative. The isotherms between $T^*=1.0$ and 1.5 in the vicinity of the critical temperature exhibit shallow minima in the gas region, as already observed for the isotherm $T^*=1.3$ in the preceding section. These results suggest that the minima are real physical effects. At lower temperatures, the gas isotherms become shorter as the dew density decreases with temperature and they decrease monotonically with density. On higher supercritical isotherms, the minima vanish, so that $D^*\rho^*$ decreases monotonically. Along an isotherm, $D^*\rho^*$ never exceeds the zero-density value. At high-density liquid states, the isotherms decrease over the whole temperature range. Below the critical density, the isotherms have concave curvature, whereas in the high-density region the curvature is convex.

At low and intermediate densities, the behavior of $D^*\rho^*$ is similar to that of the viscosity contribution η^*_{kk}, which was discussed in paper I. Close to the freezing line, the behavior is different. The η^*_{kk} isotherms are flat in this state region, and their curvature is concave.

Figure 6 shows the results for $D^*\rho^*$ along selected isochors as a function of temperature. In this representation, the range of the isochors is limited by the zero-density values from above and the values of $D^*\rho^*$ on the freezing line from below. The dependence of $D^*\rho^*$ on temperature is monotonic over the entire density range between the zero-density limit and the freezing line. $D^*\rho^*$ increases with temperature and, thus, reflects the increased mobility of the particles at high temperatures due to their higher average

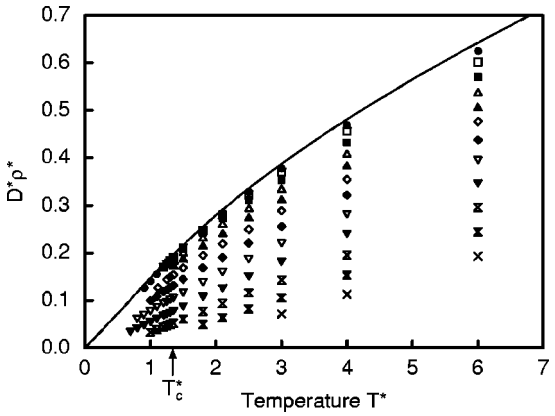

FIG. 6. $D^*\rho^*$ on selected isochors as a function of temperature. Legend: (●) $\rho^*=0.05$, (□) $\rho^*=0.1$, (■) $\rho^*=0.2$, (△) $\rho^*=0.3$, (▲) $\rho^*=0.4$, (◇) $\rho^*=0.5$, (◆) $\rho^*=0.6$, (▽) $\rho^*=0.7$, (▼) $\rho^*=0.8$, (⧖) $\rho^*=0.9$, (⧗) $\rho^*=1.0$, and (×) $\rho^*=1.1$; (—) Chapman–Enskog solution to the Boltzmann equation ($\rho^*\to 0$).

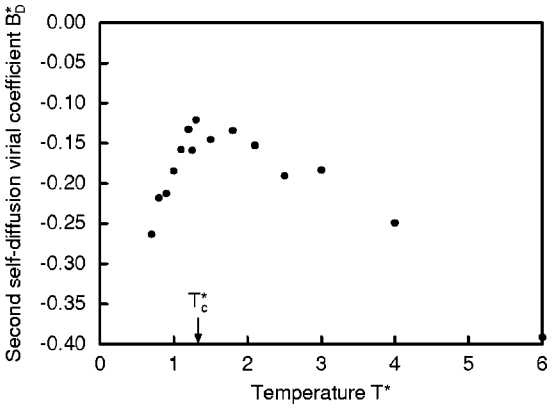

FIG. 7. The second self-diffusion virial coefficients B_D^* for the Lennard-Jones model fluid as a function of temperature.

velocities. The zero-density isochor is the steepest isochor. With increasing density the slopes of the isochors decrease.

For a detailed investigation of the initial behavior of the isotherms, estimates for the initial slopes were derived from the present simulation data on 15 isotherms. The isotherm $T^*=1.35$ was excluded because the data at this temperature do not extend close enough to the zero-density limit. The slopes were determined from a linear least-squares fit to the first few state points of every isotherm including the zero-density value from the Chapman–Enskog theory. Since these initial slopes are derived in a very simple way from the simulation data, they are of qualitative nature and might be subject to future adjustment.

The initial slopes correspond to the second self-diffusion virial coefficients that appear as coefficients of the linear term in the density expansion of $D^*\rho^*$ at low densities:[41,42]

$$D^*\rho^*=(D^*\rho^*)_0+B_D^*(T^*)\rho^*+\cdots. \tag{3}$$

Figure 7 depicts the second self-diffusion virial coefficient as a function of temperature. Despite the scatter of the data, the qualitative temperature dependence of B_D^* is evident. The second self-diffusion virial coefficients are negative over the whole temperature range between $T^*=0.7$ and $T^*=6.0$. At subcritical temperatures, B_D^* increases with temperature, reaches a maximum at $\approx T^*=1.5$, and decreases at higher temperatures. This temperature dependence is similar to that of the second viscosity virial coefficients of real fluids.[43–45]

Bennett and Curtiss[46] calculated the second self-diffusion virial coefficient for the Lennard-Jones model fluid numerically from the solution of a modified Boltzmann equation. They found that B_D^* is negative at all temperatures, approaching zero in the high-temperature limit, and reported the values $B_D^*=-3.982$, -0.9536, and -0.7240 at the temperatures $T^*=1$, 2, and 8, respectively. Within their approximative theory, B_D^* has a monotonic temperature dependence. However, the treatment of Bennett and Curtiss lacks more recent contributions to the theory by Rainwater and Friend,[43] which improve the description of several effects previously treated less rigorously. This might be the reason for the discrepancy to the present results.

VI. VELOCITY AUTOCORRELATION FUNCTIONS

The decay of velocity autocorrelation functions provides insights into the diffusion mechanisms on the molecular scale. Since the self-diffusion coefficient is related to the time integral of the velocity autocorrelation function, Eq. (1), the details of the decay influence the temperature and density dependence of $D^*\rho^*$. The discussion in this section focuses on normalized velocity autocorrelation functions at the same state points for which the shear-stress correlation functions were discussed in paper I. In some instances, time derivatives, or double logarithmic representations of the velocity autocorrelation functions, are given to illustrate their decay behavior. The representation is chosen so that the effects are optimally visible.

Figure 8 shows the initial behavior of normalized velocity autocorrelation functions and their time derivatives at low densities in the gas region. At low temperatures, the decay of the autocorrelation functions is superimposed by small oscillations that decay after a few cycles. The oscillations are clearly evident in the time derivatives of the velocity autocorrelation functions. The strongest effect is observed for the temperature $T^*=0.7$, close to the triple-point temperature. The magnitude of the oscillations increases with density, while the overall decay of the autocorrelation function becomes faster. Along the isochor $\rho^*=0.025$, the oscillations become smaller with increasing temperature and vanish for the highest temperatures displayed in Fig. 8. Moreover, the velocity autocorrelation functions decay more rapidly with increasing temperature.

Similar observations were reported by Michels and Trappeniers[33] for velocity autocorrelation functions of the Lennard-Jones model fluid at the temperatures $T^*=1.0$ and 1.5. Additionally, Michels and Trappeniers found the same effect in the velocity autocorrelation function for a system of particles interacting by a square-well potential. They attributed the oscillations to the formation of bound states at low temperatures since the effect was observed only for intermolecular potential functions with attractive forces.

Michels and Trappeniers[33] explained the occurrence of oscillations by pointing out that the velocity autocorrelation function is the scalar product of the velocity vector at the time origin and the velocity vector at a later time t and, thus, closely related to the angle between the two vectors. For example, in the case of dimers, internal vibrations and rotations of the dimer relative to its center of mass introduce periodic components into the motions of the particles that superimpose their translational motion. In an undisturbedly vibrating dimer, the relative velocity of the two molecules is reversed within half of an oscillation period resulting in a negative contribution to the velocity autocorrelation function. In the following half period, the relative velocities return to their initial value, yielding a positive contribution. Due to the permanent creation and destruction of bound states by collisions with other particles and the existence of a whole spectrum of rotational and vibrational frequencies, the oscillations in the velocity autocorrelation functions are damped out rapidly.

Dufty and Gubbins[47] and Marchetti and Dufty[48] calculated the short-time behavior of the velocity autocorrelation

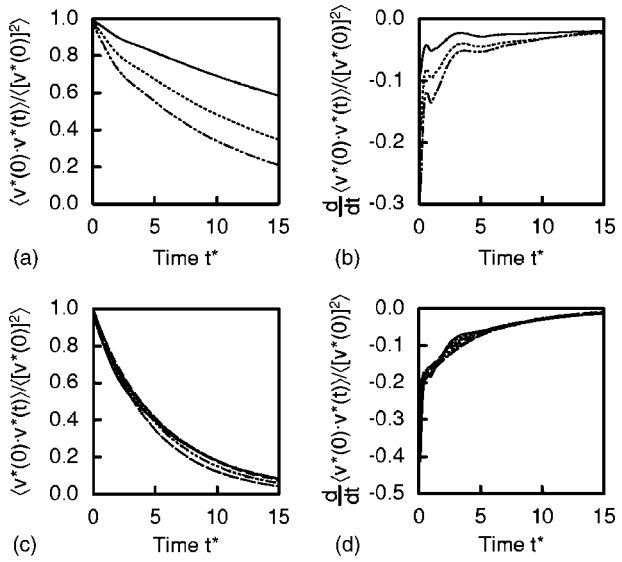

FIG. 8. Short-time behavior of the normalized velocity autocorrelation function and its time derivative at gaseous densities. (a) and (b) Density dependence on the lowest isotherm $T^*=0.7$. Legend: (—) $\rho^*=0.005$, (· · · ·) $\rho^*=0.01$, and (–··–··–) $\rho^*=0.015$. (c) and (d) Temperature dependence along the isochor $\rho^*=0.025$. Legend: (—) $T^*=0.8$, (· · · ·) $T^*=0.9$, (—·—·—·—) $T^*=1.1$, (— — —) $T^*=1.5$, (-···-··-) $T^*=2.5$, and (---·) $T^*=4.0$.

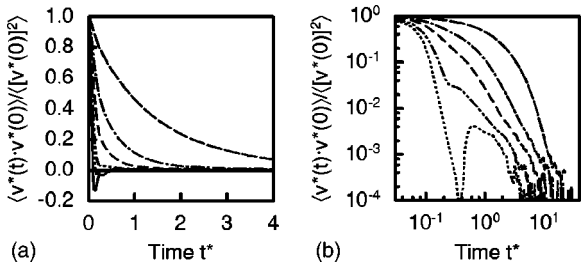

FIG. 9. Dependence of the normalized velocity autocorrelation function on density along the near-critical isotherm $T^*=1.35$ in (a) linear and (b) double logarithmic representation. Legend: (—) $\rho^*=0.95$, (· · · ·) $\rho^*=0.8$, (-··-·--·--) $\rho^*=0.7$, (---·) $\rho^*=0.5$, (—·—·—·—) $\rho^*=0.3$, and (---·) $\rho^*=0.1$.

function at low densities by means of kinetic theory for the square-well fluid. In their theory, the correlation function was separated into contributions due to scattering and bound states. The bound-state contribution showed damped oscillations, whereas the scattering contribution decayed monotonically. The superimposed result was in excellent agreement with the simulation results of Michels and Trappeniers.[33]

Since the integral of the velocity autocorrelation function determines the self-diffusion coefficient, the latter is influenced by the formation of bound states. Michels and Trappeniers[33] suggested that the formation of bound states also has an influence on the second self-diffusion virial coefficients because at low densities the number of dimers is proportional to density.[49] This hypothesis is supported by the Rainwater–Friend theory[43] which shows that bound states have an influence on the second viscosity and thermal conductivity virial coefficient. A quantification of the effect would require an extension of the Rainwater–Friend theory to self-diffusion.

The decay behavior of the velocity autocorrelation closely resembles the behavior of the kinetic-kinetic shear-stress correlation functions at low densities discussed in paper I. However, this is not surprising since both correlation functions measure correlations between particle velocities. Moreover, the dependence of $D^*\rho^*$ and the viscosity contribution η^*_{kk} on density and temperature at low densities is similar. Superimposed oscillations were also observed in paper I in the decay of the kinetic-potential, and potential-potential shear-stress correlation functions with the same temperature and density dependence as found here for the velocity autocorrelation functions.

Figure 9 shows the dependence of the normalized velocity autocorrelation function on density for the supercritical isotherm $T^*=1.35$. At low and intermediate densities, the velocity autocorrelation function decays slowly, whereas in the liquid region it decays rapidly to negative values, exhibits a minimum and increases to positive values. Close to the freezing line at the density $\rho^*=0.95$, several oscillations are observed in the negative regime. This behavior is known as the backscattering effect, see, for example, Refs. 50 and 51. It was examined in detail by Rahman.[52] By molecular-dynamics simulations with an argonlike potential at a high-density liquid state, Rahman resolved the behavior of a particle within the cagelike structure formed by its neighboring particles in the liquid. He found that the particle moves preferably in that direction where the neighboring particles of the first shell are farthest apart from the particle and thus provide free space for the particle to diffuse to. In the plane perpendicular to this direction, the particle may oscillate several times back and forth before the correlations vanish. This latter effect mainly causes the negative regime and oscillating behavior of the velocity autocorrelation function.

The decay of the velocity autocorrelation functions at high densities differs from that of the kinetic-kinetic shear-stress correlation functions described in paper I. The kinetic-kinetic shear-stress correlation functions do not show the negative regime found for the velocity autocorrelation functions in this state region. This difference yields the explanation for the different behavior of the $D^*\rho^*$ and η^*_{kk} isotherms at high densities (Figs. 4 and 5 of this work and Fig. 9 of paper I). The negative regime of the velocity autocorrelation function lowers the values of $D^*\rho^*$ so that the isotherms are relatively steep at high densities. On the other hand, the η^*_{kk} isotherms are flat in this state region, which is a consequence of the monotonic decay of the kinetic-kinetic shear-stress correlation functions (Fig. 17 in paper I).

The long-time behavior of the autocorrelation functions is better assessed in the double logarithmic representation. It is evident that the velocity autocorrelation function always approaches the time axis asymptotically from above. At long times, the decay is linear in double logarithmic representation before it vanishes in random noise for values of the autocorrelation functions below 0.001. This linear long-time behavior corresponds to hyperbolic decay of the type $\sim t^{-m}$ in the linear representation. The exponent $-m$ is the slope of the linear decay in the double logarithmic representation. The slope depends on the density of the state point and in-

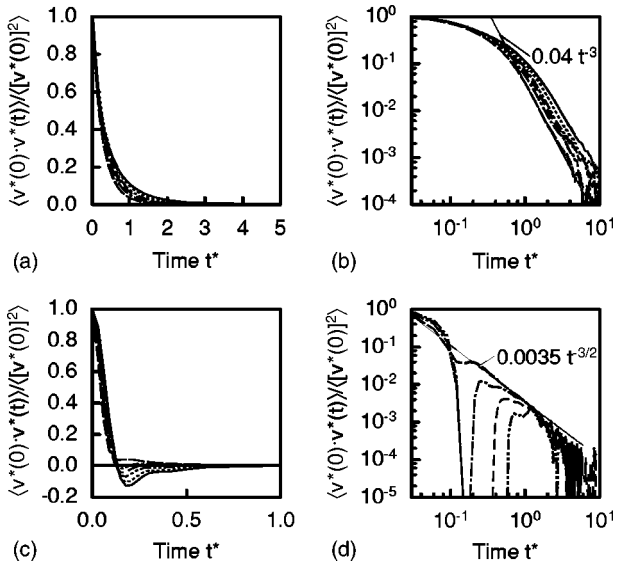

FIG. 10. Dependence of the normalized velocity autocorrelation function on temperature in linear and double logarithmic representation. (a) and (b) Along the isochor $\rho^*=0.3$ close to the critical density. Legend: (—) $T^*=1.358$, (· · · ·) $T^*=1.8$, (-···-···-) $T^*=2.5$, (---·) $T^*=3.0$, (—·—·—·—) $T^*=4.0$, and (---·) $T^*=6.0$. (c) and (d) Along the liquid isochor $\rho^*=0.85$. Legend: (—) $T^*=0.7$, (· · · ·) $T^*=0.9$, (-···-···-) $T^*=1.3$, (---·) $T^*=1.8$, (—·—·—·—) $T^*=2.5$, and (---·) $T^*=6.0$. Negative values of the autocorrelation functions are not shown in the double logarithmic plots.

creases towards lower densities. Numerical values of the slopes were determined by linear-least-squares fits to the linear long-time parts of the velocity autocorrelation functions in the double logarithmic representation. The slopes are -1.4, -1.95, -2.5, and -4.8 at the densities $\rho^*=0.7$, 0.5, 0.3, and 0.1, respectively.

Hyperbolic long-time tails in the velocity autocorrelation functions were first observed by Alder and Wainwright[53,54] for a hard-sphere fluid and, subsequently, explained by theoretical investigations using mode coupling approaches and kinetic theory.[55–57] In contrast to the present results for the long-time tail exponents, Alder and Wainwright found the value $-3/2$ for the hard-sphere fluid independent of the density of the state point. Alder and Wainwright[54,58] explained the long-time decay of the velocity autocorrelation function by a simple hydrodynamic model. This hydrodynamic model treats the motion of a spherical particle with a prescribed initial velocity through a continuum liquid that represents the surrounding particles. The forward movement of the spherical particle creates a vortex. After about ten collisions, the vortex has the size of three particle diameters and feeds the velocity of the spherical particle back into itself via the surrounding medium. This effect leads to the long-time correlations.

Figure 10 depicts the normalized velocity autocorrelation functions for the two isochors $\rho^*=0.3$ and $\rho^*=0.85$ for several temperatures. Along the close-critical isochor $\rho^*=0.3$, the decay becomes faster with increasing temperature. Due to the higher average velocity of the particles, collisions occur more frequently, which causes the correlations to decay more rapidly. Therefore, the integral of the normalized velocity autocorrelation function decreases with temperature, and the increase of $D^*\rho^*$ is caused by the initial value of the correlation function $\langle \mathbf{v}_i^2 \rangle$. As $\langle \mathbf{v}_i^2 \rangle$ is related to the temperature by the equipartition theorem,[13] the temperature itself is the cause for the increase of $D^*\rho^*$. In double logarithmic representation, the linear long-time regime is evident for every displayed temperature at this isochor. The long-time tails are almost parallel, with exponents of about -3.

At the higher liquid isochor $\rho^*=0.85$, the behavior is different. The negative region at intermediate times is shifted above the time axis with increasing temperature, thus, increasing the integral under the normalized autocorrelation function. At this density, the increase of $D^*\rho^*$ is due to temperature as well as to the slower decay of the normalized autocorrelation function. In double logarithmic representation, the autocorrelation function at the highest displayed temperature $T^*=6.0$ reaches the linear long-time behavior after the negative regime and follows closely the curve $0.0035t^{-3/2}$. The exponent from a linear-least-squares fit to the double logarithmic representation is -1.54. At lower temperatures, the linear long-time tails are not observable before the autocorrelation functions vanish in the noise. However, a consequent continuation of the previously described behavior to low temperatures would support the existence of the long-time tails after the negative regime.

The results of this section for the long-time behavior of the velocity autocorrelation functions suggest that the exponent of the long-time tail depends on the density of the state point. Only at liquid densities, the present results agree with the theoretically predicted value $-3/2$. With decreasing density, the hyperbolic decay at long times persists, but the exponent becomes larger. This behavior is not unreasonable because it is expected that there is a continuous transition to the zero-density limit.

Hyperbolic long-time tails in velocity autocorrelation functions with exponents $-3/2$ were mainly found for hard- and soft-sphere model fluids, in which the particles interact by repulsive forces only.[53,58] At high liquid densities, where we find long-time tails with exponents $-3/2$, the properties of the Lennard-Jones model fluid are also dominated by the repulsive forces between the particles. However, with decreasing density, where we observe hyperbolic decay with larger negative exponents, the influence of the attractive part of the Lennard-Jones potential increases. It is likely that the slow hyperbolic decay with exponent $-3/2$ at long times is only observed if the forces between the fluid particles are purely repulsive. If long-time tails at low and intermediate densities in the Lennard-Jones model fluid are observable, they must occur at greater times than those considered in this work.

Very recently, McDonough *et al.*[59] investigated the long-time behavior of the velocity autocorrelation functions of the Lennard-Jones and soft-sphere model fluid with systems of 4000 particles at the reduced temperature $T^*=2.17$. They found that long-time tails with the exponent $-3/2$ are observable for both models after 2.57 and 2.1 reduced time units at the reduced densities $\rho^*=0.35$ and $\rho^*=0.55$, respectively. However, a closer inspection of their results (Figs. 1 and 3 in Ref. 59) shows that in this time regime noise dominates the velocity autocorrelation functions, so

that their conclusion in our view appears questionable. For $\rho^* < 0.15$, McDonough *et al.* found that the long-time behavior of the velocity autocorrelation function is well approximated by an exponential decay. At liquid densities $\rho^* > 0.55$, they could not assess the long-time behavior within the accuracy of their simulations. This may be due to the reduced temperature $T^* = 2.17$ of their simulations. The present results clearly show the hyperbolic decay with exponent $-3/2$ at the higher temperature $T^* = 6.0$, but we also found it difficult to observe it at much lower temperatures.

The results for the long-time behavior of the velocity autocorrelation function raise the question of whether the slow decay has an impact on the accuracy of the self-diffusion data. Since the fit interval in the Einstein plots is always chosen in the linear regime, it is ensured that all correlations have decayed to a negligible level. For example, at densities above $\rho^* = 0.7$ the start of the fit interval was usually chosen at $t^* = 6.0$ or later, where the long-time tails have vanished in the noise. Therefore, systematic errors of the present data due to long-time tails are not expected.

VII. CONCLUSIONS

Thermophysical properties of model fluids are important references for developing an understanding of the behavior of real fluids. The Lennard-Jones potential describes interactions between spherical nonpolar molecules and is an important model in many applications of statistical thermodynamics. In this work, the self-diffusion coefficient of the Lennard-Jones model fluid was determined by equilibrium molecular-dynamics simulations using the Einstein-relation method. About 330 data cover a large part of the fluid region from the low-density gas to the compressed liquid close to the freezing line in the temperature range between $T^* = 0.7$ close to the triple-point temperature and $T^* = 6.0$ (about 4.5 times the critical temperature). It was found that the self-diffusion coefficient shows a strong dependence on the number of particles in the simulated system. By using systems larger than in previous studies, the present data based on 1372 particles are significantly closer to the infinite-system size values. The accuracy of the present data is estimated to be 0.5% in the liquid region and 1% at gaseous states. The high accuracy of the data is demonstrated by comparisons with literature data. With this comprehensive data set, the temperature and density dependence of the product self-diffusion coefficient times density $D^*\rho^*$ is characterized. In particular, the previously little-investigated behavior at low-density gaseous states was analyzed in detail. Furthermore, an analysis of the velocity autocorrelation functions yielded some insights into the mass transport mechanisms on the molecular scale and helped in explaining the temperature and density dependence of $D^*\rho^*$. In this context, the influence of the formation of bound states at low-temperature gaseous states on the self-diffusion coefficient was discussed, and the decay behavior of the velocity autocorrelation function at long times was examined over a wide range of fluid states. Within the considered time domains and statistical errors, it was found that the velocity autocorrelation function decays hyperbolically at long times, with the exponent of the decay depending strongly on the density of the state point. Only at high liquid densities, the theoretically predicted hyperbolic decay with exponent $-3/2$ was observed.

ACKNOWLEDGMENTS

K.M. acknowledges an appointment as a guest researcher at the Physical and Chemical Properties Division of the National Institute of Standards and Technology in Boulder during summer 1999, where parts of this research were carried out. Computational resources for this work were provided by the Regional Computing Center for Lower Saxony at the University of Hannover (RRZN), the Konrad-Zuse-Zentrum for Information Technology in Berlin, and the NIST Information Technology Laboratory in Gaithersburg. We acknowledge the assistance of Dr. Simone Knief and Jürgen Fischer (RRZN) with the parallelization of the software, and the assistance of Denis Lehane at NIST.

[1] K. Meier, A. Laesecke, and S. Kabelac, Int. J. Thermophys. **22**, 161 (2001).
[2] K. Meier, *Computer Simulation and Interpretation of the Transport Coefficients of the Lennard-Jones Model Fluid* (Shaker, Aach, 2002).
[3] K. Meier, A. Laesecke, and S. Kabelac, J. Chem. Phys. **121**, 3671 (2004).
[4] K. Meier, A. Laesecke, and S. Kabelac, J. Chem. Phys. (to be published).
[5] K. Meier, A. Laesecke, and S. Kabelac (unpublished).
[6] P. H. Oosting and N. J. Trappeniers, Physica (Utrecht) **51**, 418 (1971); K. R. Harris and N. J. Trappeniers, Physica A **104**, 262 (1980); B. Arends, K. O. Prins, and N. J. Trappeniers, *ibid.* **107**, 307 (1981); P. W. E. Peereboom, H. Luigjes, K. O. Prins, and N. J. Trappeniers, Physica B **139 & 140**, 134 (1986).
[7] F. X. Prielmeier, E. W. Lang, and H.-D. Lüdemann, Mol. Phys. **52**, 1105 (1984); F. X. Prielmeier and H.-D. Lüdemann, *ibid.* **58**, 593 (1986); E. W. Lang, F. X. Prielmeier, H. Radkowitsch, and H.-D. Lüdemann, Ber. Bunsenges. Phys. Chem. **91**, 1017 (1987).
[8] P. W. E. Peereboom, H. Luigjes, and K. O. Prins, Physica A **156**, 260 (1989).
[9] K. R. Harris, Physica A **94**, 448 (1978).
[10] H. Liu, C. M. Silva, and E. A. Macedo, Chem. Eng. Sci. **53**, 2403 (1998).
[11] R. Zwanzig, Annu. Rev. Phys. Chem. **16**, 67 (1965).
[12] J. R. Ray and H. Zhang, Phys. Rev. E **59**, 4781 (1999).
[13] M. P. Allen and D. J. Tildesley, *Computer Simulation of Liquids* (Clarendon, Oxford, 1987).
[14] J. J. Erpenbeck, Phys. Rev. E **51**, 4296 (1995).
[15] J. O. Hirschfelder, C. F. Curtiss, and R. B. Bird, *Molecular Theory of Gases and Liquids* (Wiley, New York, 1954).
[16] R. Friedberg and J. E. Cameron, J. Chem. Phys. **52**, 6049 (1970).
[17] See EPAPS Document No. E-JCPSA6-121-521435 for text files with tabulated simulation results and larger colored figures of this article. A direct link to this document may be found in the online article's HTML reference section. The document may also be reached via the EPAPS homepage (http://www.aip.org/pubservs/epaps.html) or from ftp.aip.org in the directory /epaps/. See the EPAPS homepage for more information.
[18] ftp://FTP.Boulder.NIST.Gov/pub/fluids/Lennard-Jones
[19] P. Borgelt, C. Hoheisel, and G. Stell, Phys. Rev. A **42**, 789 (1990).
[20] M. Canales and J. A. Padró, Phys. Rev. E **60**, 551 (1999).
[21] S.-H. Chen and A. Rahman, Mol. Phys. **34**, 1247 (1977).
[22] J. J. Erpenbeck, Phys. Rev. A **35**, 218 (1987).
[23] J. J. Erpenbeck, Phys. Rev. A **38**, 6255 (1988).
[24] P. J. Gardner, D. M. Heyes, and S. R. Preston, Mol. Phys. **73**, 141 (1991).
[25] K. D. Hammonds and D. M. Heyes, J. Chem. Soc., Faraday Trans. 2 **84**, 705 (1988).
[26] D. M. Heyes, J. Chem. Soc., Faraday Trans. 2 **79**, 1741 (1983).
[27] D. M. Heyes, J. Chem. Soc., Faraday Trans. 2 **83**, 1985 (1987).
[28] D. M. Heyes, Phys. Rev. B **37**, 5677 (1988).
[29] D. M. Heyes and J. G. Powles, Mol. Phys. **71**, 781 (1990).
[30] D. M. Heyes, J. G. Powles, and J. G. Gil Montero, Mol. Phys. **78**, 229 (1993).
[31] J. M. Kincaid, R.-F. Tuo, and M. L. de Haro, Mol. Phys. **81**, 837 (1994).
[32] J. A. Leegwater, J. Chem. Phys. **94**, 7402 (1991).

[33] J. P. J. Michels and N. J. Trappeniers, Chem. Phys. Lett. **33**, 195 (1975).
[34] J. P. J. Michels and N. J. Trappeniers, Physica A **90**, 179 (1978).
[35] R. L. Rowley and M. M. Painter, Int. J. Thermophys. **18**, 1109 (1997).
[36] P. Schofield, Comput. Phys. Commun. **5**, 17 (1973).
[37] S. Sharma, Ph.D. thesis, Chemical Engineering Department, University of Bradford, 1994.
[38] J. E. Straub, Mol. Phys. **76**, 373 (1992).
[39] D. M. Heyes, Can. J. Phys. **64**, 773 (1986).
[40] D. J. Evans, G. P. Morriss, and L. M. Hood, Mol. Phys. **68**, 637 (1989).
[41] R. Zwanzig, Phys. Rev. **129**, 486 (1963).
[42] K. Kawasaki and I. Oppenheim, Phys. Rev. **139**, A1763 (1965).
[43] J. C. Rainwater, J. Chem. Phys. **81**, 495 (1984); D. G. Friend and J. C. Rainwater, Chem. Phys. Lett. **107**, 590 (1984); J. C. Rainwater and D. G. Friend, Phys. Rev. A **36**, 4062 (1987).
[44] E. Bich and E. Vogel, in *Transport Properties of Fluids: Their Correlation, Prediction and Estimation*, edited by J. Millat, J. H. Dymond, and C. A. Nieto de Castro (Cambridge University Press, Cambridge, 1996), pp. 72–82.
[45] B. Najafi, Y. Ghayeb, J. C. Rainwater, S. Alavi, and R. F. Snider, Physica A **260**, 31 (1998).
[46] D. E. Bennett and C. F. Curtiss, J. Chem. Phys. **51**, 2811 (1969).
[47] J. W. Dufty and K. E. Gubbins, Chem. Phys. Lett. **64**, 142 (1979).
[48] M. C. Marchetti and J. W. Dufty, Chem. Phys. Lett. **70**, 539 (1980); Phys. Rev. A **24**, 2116 (1981).
[49] D. E. Stogryn and J. O. Hirschfelder, J. Chem. Phys. **31**, 1531 (1959).
[50] J. Kushick and B. J. Berne, J. Chem. Phys. **59**, 3732 (1973).
[51] J. P. Boon and S. Yip, *Molecular Hydrodynamics* (McGraw-Hill, New York, 1980).
[52] A. Rahman, J. Chem. Phys. **45**, 2585 (1966).
[53] B. J. Alder and T. E. Wainwright, Phys. Rev. Lett. **18**, 988 (1967).
[54] B. J. Alder and T. E. Wainwright, Phys. Rev. A **1**, 18 (1970).
[55] M. H. Ernst, E. H. Hauge, and J. M. J. van Leeuwen, Phys. Rev. A **4**, 2955 (1971); J. Stat. Phys. **15**, 7 (1976); *ibid.* **15**, 23 (1976).
[56] Y. Pomeau and P. Résibois, Phys. Rep. **19**, 63 (1975).
[57] P. Résibois and M. De Leener, *Classical Kinetic Theory of Fluids* (Wiley, New York, 1977).
[58] B. J. Alder and W. E. Alley, Phys. Today **37**, 56 (1984).
[59] A. McDonough, S. P. Russo, and I. K. Snook, Phys. Rev. E **63**, 6109 (2001).